Research on Fault Location Method in Distribution Network with DG Based on PADEA

Zhongjian Kang[1], Ruiying Liu[1], and Yanyan Feng[2]
[1] College of Information and Control Engineering, China University of Petroleum, Qingdao 266580, China
[2] Zaozhuang Power Supply Bureau, Zaozhuang 277000, China
Email: {kangzjzh, 18266632686}@163.com; 919630086 @qq.com

Abstract— For better solving the problem of multi-terminal fault location in the distribution network, this paper proposes a new fault location method based on Strong Tracking Filter (STF) and Parameter Adaptive Differential Evolution Algorithm (PADEA), which can be applied to asynchronous sampling systems. STF is adopted for real-time fundamental wave amplitudes' extraction of voltage and current. STF can achieve the fast track of power parameters' mutation, and also make the construction of the Distributed Generators' (DG) impedance model more accurate. On the basis of the establishment of impedance model and fault feature analysis, the fault feature value is defined by using only the amplitude of signals measured at the measurement points without introducing the phase angle, which can avoid the introduction of the sampling error radically. PADEA is adopted in the precise fault location part. The use of PADEA can improve the simulation efficiency and result accuracy. Simulation results in MATLAB/Simulink show that the method proposed in this paper has advantages of high accuracy and strong robustness.

Index Terms—Strong Tracking Filter (STF), fault location, Parameter Adaptive Differential Evolution Algorithm (PADEA), asynchronous sampling

I. Introduction

The research on fault location has always been an important issue for the power system [1]. Most of the present fault location methods can only be applied in synchronous sampling systems without taking the error of actual signals into account. Fault recorders are connected to the Internet in distribution system, though the measured data can't meet the required synchronous condition. In recent years, most asynchronous fault location methods adopted the way of constructing and solving nonlinear optimal equations. And existing methods which are suitable for asynchronous sampling system mostly focus on how to eliminate the synchronous angle, such as constructing nonlinear equations [2]-[4], estimating or eliminating the asynchronous angle [5], [6]. However, these methods can't eliminate entirely the influence of asynchronous angle on fault location result radically.

To solve the above-mentioned problem, this paper presents a new fault location method applied to asynchronous sampling system based on STF and PADEA.

Manuscript received June 24, 2015; revised August 19, 2015.
Project Supported by National Natural Science Foundation of China (61271001) and the Fundamental Research Funds for the Central Universities of China under Grant No. 14CX05039A.
Corresponding author email: kangzjzh@163.com
doi:10.12720/jcm.10.8.621-628

II. Fault Characteristic Analysis of Distribution Network Based on Impedance Model

A. The Establishment of Distribution Network Impedance Model

According to the topological structure and corresponding parameters of the system, the node admittance matrix of system is shown in (1), which can be obtained by [7].

$$Y_{abc}=\begin{bmatrix} Y_{11} & Y_{12} & \cdots & Y_{1n} \\ Y_{21} & Y_{22} & \cdots & Y_{2n} \\ \vdots & \vdots & \vdots & \vdots \\ Y_{n1} & Y_{n2} & \cdots & Y_{nn} \end{bmatrix}_{3n\times 3n} \tag{1}$$

Here, Y_{nn} is the self-impedance of the n^{th} node; Y_{nm} is the mutual impedance between the n^{th} node and the m^{th} node.

The three-phase unbalanced node admittance equation [8] of the distribution network with n nodes is shown in (2).

$$\begin{bmatrix} Y_{11} & Y_{12} & \cdots & Y_{1n} \\ Y_{21} & Y_{22} & \cdots & Y_{2n} \\ \vdots & \vdots & \vdots & \vdots \\ Y_{n1} & Y_{n2} & \cdots & Y_{nn} \end{bmatrix}_{3n\times 3n} \times \begin{bmatrix} V_1 \\ V_2 \\ \vdots \\ V_n \end{bmatrix}_{3n\times 1} = \begin{bmatrix} I_1 \\ I_2 \\ \vdots \\ I_n \end{bmatrix}_{3n\times 1} \tag{2}$$

Here $V_i=\begin{bmatrix} V_{ia} \\ V_{ib} \\ V_{ic} \end{bmatrix}$ and $I_i=\begin{bmatrix} I_{ia} \\ I_{ib} \\ I_{ic} \end{bmatrix}$ are the three-phase node voltages and injection currents of the i^{th} node.

The node impedance matrix and the node admittance matrix are mutually inverse matrix.

Thus, a three-phase impedance model which considers the asymmetry of the distribution network with DG has been established.

B. Fault Feature Analysis

Assuming that the number of power points including one main source and DGs is *m*, the power points are respectively defined as $BS(1), BS(2)\cdots BS(m)$, the fault location is at j^{th} node, the voltage and injection current of each power point can be measured. The pre-fault measured

voltage vectors at each power point are respectively defined as $\dot{V}_{BS}(1),\dot{V}_{BS}(2)\cdots\dot{V}_{BS}(m)$, and the measured voltage vectors at each power point in fault are respectively defined as $\dot{V}_{BS}'(1),\dot{V}_{BS}'(2)\cdots\dot{V}_{BS}'(m)$.

Each fault voltage components ΔV generated by short circuit current vector $\dot{I}_{fj}$ at the fault node is shown in the formula (3).

$$\begin{bmatrix}\Delta V_1\\ \vdots\\ \Delta V_j\\ \vdots\\ \Delta V_1\end{bmatrix}=\begin{bmatrix}Z_{11} & \cdots & Z_{1j} & \cdots & Z_{1n}\\ \vdots & \cdots & \vdots & \cdots & \vdots\\ Z_{j1} & \cdots & Z_{jj} & \cdots & Z_{jn}\\ \vdots & \cdots & \vdots & \cdots & \vdots\\ Z_{n1} & \cdots & Z_{nj} & \cdots & Z_{nn}\end{bmatrix}\begin{bmatrix}0\\ \vdots\\ -\dot{I}_{fj}\\ \vdots\\ 0\end{bmatrix} \tag{3}$$

In (3), the fault voltage component ΔV_i can be calculated by the difference between the voltage vector in fault and pre fault shown as (5).

So the fault current of the j^{th} node can be calculated through (4-5).

$$\Delta V_i=-Z_{ij}\dot{I}_{fj}(i=1,2\cdots m) \tag{4}$$

$$\dot{I}_{fj}(i)=-\frac{\dot{V}_{BS}'(i)-\dot{V}_{BS}(i)}{Z_{ij}}(i=1,2\cdots m) \tag{5}$$

Here, *j* represents the location number of the assumed fault point; *i* represents the location number of the measurement point.

Because the fault currents calculated by fault voltage component at different power measuring points should be the same vector, the cumulative error between the fault current calculated by different power supplies is defined as the fault feature value, as shown in (6).

$$E(j)=\sum_{i=1}^{m-1}\left|\dot{I}_{fj}(i)-\dot{I}_{fj}(i+1)\right| \tag{6}$$

However, the vector will introduce the asynchronous angle between different measurements. To avoid the asynchronous influence, the calculation of current phasors in (6) can be changed to magnitude calculation as the phasors are approximately equal and then the magnitudes of the signals will also be approximately equal.

$$E(j)=\sum_{i=1}^{m-1}\left|I_{fj}(i)-I_{fj}(i+1)\right| \tag{7}$$

According to the electrical network theory, the fault current at fault point calculated by one power source is equal to that calculated by another one. When the assumed fault point is exactly the point of the actual failure, the fault feature value should be smallest among all calculated feature value. Hence, a node with the smallest feature value is the associated node of fault branch. As the clock at the same measurement point is the same, there is not any asynchronous problem.

III. Fault Location in Distributed Network with DG based on PADEA

A two-step method is given in this paper, which includes fault area location based on the enumeration method and fault precise location based on PADEA.

A. Fault Area Location Method Based on STF

1) Real-time extraction of voltage fundamental phase based on STF

Strong tracking filter (STF) [9], [10] is adopted in this method for real-time extraction of fundamental wave's phase and amplitude of voltage and current, and to fast track the power parameters mutation, which makes the DG impedance model and the location results more accurate.

Discrete form of single phase voltage signal can be expressed as

$$y_k=\sum_{n=1}^{N}A_n\sin\left(k\omega_nT_s+\varphi_n\right)+v_k,N=1,2\cdots \tag{8}$$

Here, A_n and φ_n is respectively the n-th sinusoidal component amplitude and initial phase angle in single-phase voltage signal. ω_n is the frequency of the n-th sinusoidal component, T_s is sampling time interval, v_k is the white Gaussian noise added to the single phase voltage.

Assumes that the single phase voltage signal contains only fundamental component, equation (8) can be simplified as follows:

$$\begin{aligned}y_k&=A_1\sin(k\omega_1T_s+\varphi_1)\\&=(-0.5j)(A_1e^{j(k\omega_1T_s+\varphi_1)})+(0.5j)(A_1e^{-j(k\omega_1T_s+\varphi_1)})\end{aligned} \tag{9}$$

The state variable of voltage signal is defined as

$$\begin{bmatrix}x_{1k}\\ x_{2k}\\ x_{3k}\end{bmatrix}=\begin{bmatrix}e^{j\omega_1T_s}\\ A_1e^{j(\omega_1T_s+\varphi_1)}\\ A_1e^{-j(\omega_1T_s+\varphi_1)}\end{bmatrix} \tag{10}$$

Here, ω_1 is fundamental frequency; A_1 is the fundamental amplitude, φ_1 is the fundamental initial phase.

Therefore, the nonlinear state space description of voltage signal is given by (11).

$$\begin{aligned}x_{k+1}&=f(x_k)+\omega_k\\ y_k&=Hx_k+\upsilon_k\end{aligned} \tag{11}$$

Here: $x=\begin{bmatrix}x_1 & x_2 & x_3\end{bmatrix}^T;f(\mathrm{x}_k)=\begin{bmatrix}x_{1k} & x_{1k}x_{2k} & x_{3k}/x_{1k}\end{bmatrix}^T$, $H=\begin{bmatrix}0 & -0.5j & 0.5j\end{bmatrix}$. Excitation process noise w_k and measurement noise v_k satisfy the condition in [10].

When voltage signal contains harmonic components, state variables can be expanded. For example, if voltage signal contains the fifth harmonic, (12) can be added to the state variables defined in (10).

$$\begin{bmatrix}x_{4k}\\ x_{5k}\end{bmatrix}=\begin{bmatrix}A_5e^{j(\omega_5T_s+\varphi_5)}\\ A_5e^{-j(\omega_5T_s+\varphi_5)}\end{bmatrix} \tag{12}$$

STF can recursively estimate the state variables defined in (10), the process is shown below.

1. Prediction stage. This step is to calculate the value of the state prediction and covariance matrix of the prediction error.

The value of the state prediction is

$$\hat{x}_{k+1|k} = f\left(\hat{x}_k\right) \tag{13}$$

The covariance matrix of the prediction error is

$$P_{k+1|k} = \lambda_{k+1} F_{k+1|k} P_k F_{k+1|k}^T + Q_k \tag{14}$$

Here, $F_{k+1|k} = \dfrac{\partial f(x_k)}{\partial x_k} = \begin{bmatrix} 1 & 0 & 0 \\ x_{2k} & x_{1k} & 0 \\ -x_{3k}/x_{1k}^2 & 0 & 1/x_{1k} \end{bmatrix}; \lambda_{k+1} \geq 1$ is suboptimal fading factor. It is calculated as follows:

$$\lambda_{k+1} = \begin{cases} \lambda_0, \lambda_0 \geq 1 \\ 1, \lambda_0 < 1 \end{cases}, \lambda_0 = \frac{tr\left[N_{k+1}\right]}{tr\left[M_{k+1}\right]} \tag{15}$$

where $tr[\ ]$ is the matrix trace operator, $\beta \geq 1$ is a selected weakening factor, V_{k+1} is the covariance matrix of the actual output residuals, it is unknown in practice, and can be estimated by (16).

$$V_{k+1} = \begin{cases} \varepsilon_1 \varepsilon_1^T, k = 1 \\ \dfrac{\rho V_k + \varepsilon_{k+1} \varepsilon_{k+1}^T}{1+\rho}, k \geq 1 \end{cases} \tag{16}$$

Here, $0 \leq \rho \leq 1$ is forgetting factor, and generally $\rho = 0.95$; $\varepsilon_{k+1} = (y_{k+1} - \hat{y}_{k+1|k})$.

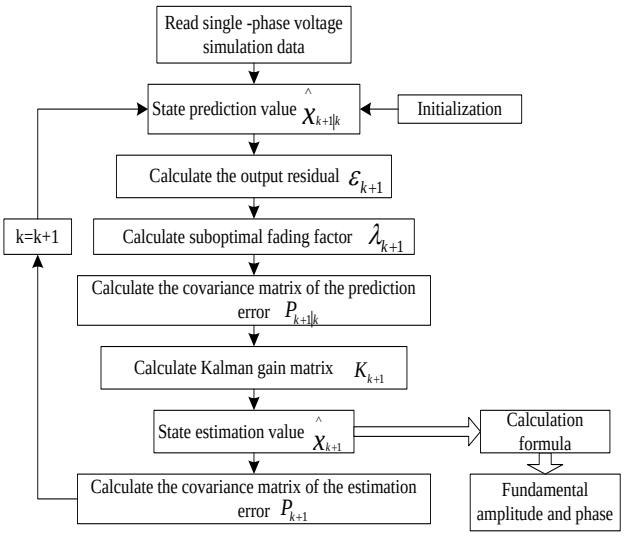

Fig. 1. The flowchart of the STF-based fundamental phase real-time extracting method for single-phase grid voltage.

2. Updating stage. This step is to calculate the constructed gain matrix, and update the state estimation value and the covariance matrix of estimation error.

The gain matrix is

$$K_{k+1} = P_{k+1|k} H^T (H P_{k+1|k} H^T + R_{k+1})^{-1} \tag{17}$$

The state estimation value is

$$\hat{x}_{k+1} = \hat{x}_{k+1|k} + K_{k+1} \varepsilon_{k+1} \tag{18}$$

Here, actual output residuals is $\varepsilon_{k+1} = (y_{k+1} - \hat{y}_{k+1|k})$, $\hat{y}_{k+1|k} = H\hat{x}_{k+1|k} + R_{k+1}$.

The covariance matrix of estimation error is

$$P_{k+1} = (I - K_{k+1} H) P_{k+1|k} \tag{19}$$

The state variable is recursively estimated with STF, by (20)-(22) the fundamental frequency, amplitude and phase at $(k+1)T_s$ can be obtained [10]. Fig. 1 is the flowchart of the STF-based fundamental phase real-time extracting method for single-phase grid voltage.

$$\hat{f}_{k+1} = \frac{1}{2\pi T_s}\left[\mathrm{Im}(\ln(\hat{x}_{1k+1}))\right] \tag{20}$$

$$\hat{A}_{1k+1} = \left|\hat{x}_{2k+1}\right| \tag{21}$$

$$\varphi_{1k+1} = \mathrm{Im}\left[\ln\left(\frac{\hat{x}_{2k+1}}{\left|\hat{x}_{2k+1} \times (\hat{x}_{1k+1})^{k+1}\right|}\right)\right] \tag{22}$$

2) The identification of potential fault area

The steps of fault area location are:

- Read in the relevant parameters of power supply, lines and load for making preparations for the establishment of impedance model;
- Adopt STF for real-time extraction of fundamental wave phase and amplitude of phase voltage and current, and fast track the power parameters mutation;
- Establish three phase impedance model according to the method introduced in [8];
- Calculate the fault feature value *E(j)* assuming the j^{th} node is the fault point according to the definition;
- Begin from the first node to the n^{th} node(the last node in the network) to calculate the corresponding fault feature values which are respectively defined as *E(1),E(2)…E(n)*;

- Select three minimum of the values for avoiding misjudgments, and name them respectively as K_1, K_2 and K_3;
- Judge out the lines which are connected with the fault associated nodes as possible fault lines.

The detailed flow chart of fault area location is shown as Fig. 2.

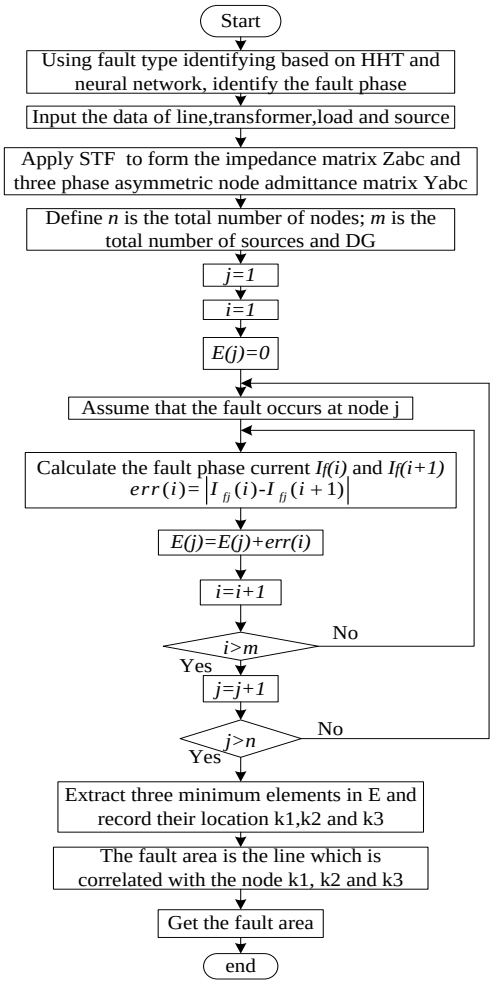

Fig. 2. Flow chart of fault area location.

B. *Precise Fault Location Method Based on Parameter Adaptive Difference Evolutionary Algorithm*

After identifying the possible fault line, the fault location needs to be accurately determined. According to the above analysis, the fault feature value at actual fault point is the smallest. Therefore this method adopts PADEA on the judged fault branch to search automatically for the fault situation which most matches the fault feature. The output is the precise fault location result.

1) Parameter adaptive differential evolution algorithm

Compared with traditional artificial intelligence algorithm, DE is a direct parallel global search based on the population differences and owns the characteristics of simple construction and ease of use [11]. However, the fixed control parameters setting and mutation strategy make the original DE owns the disadvantages such as premature and poor convergence effect. Therefore, this paper applies PADEA to modify the original fault location optimization algorithm.

The factors of differential evolution algorithm mainly include individual fitness function, differential operation and parameter settings. Among them, parameter setting is the master key in PADEA [12]-[15].

(1) Fitness function

Fitness function is the main criterion for evaluation of individual fitness, which is also the criterion for individual selection.

(2) Differential operation

Assuming that the population size is *NP*, each generation can be represented by NP D-dimensional vectors in iteration process as $X_{i,G}(i=1,2...NP)$. Then mutation operation, crossover operation, selection operation will be carried out on every individual [12].

(3) Parameter settings

The above three basic differential operations involve several parameters which will be respectively introduced in the following content.

① Population size NP

NP represents the individual number of each population. The larger size can make it easier to get optimum value but cause longer time for calculation.

②The largest iterative number *G*

The largest iterative number G in this paper is set as 50 in view of the accuracy and calculation time.

③Variation factor F

Aiming at the disadvantages of the fixed variation factor, a zoom factor F is adopted which can adjust adaptively with the change of differential vector.

④ Crossover probability *CR*

CR is often set as 0.4 through prior knowledge. When the value of *CR* is quite greater, the new individual will have a bigger contribution on the individual $U_{i,G+1}$. For example, when *CR=1*, $U_{i,G+1}= V_{i,G+1}$, it can improve convergence speed; whereas when the value of *CR* is quite smaller, the target vector individual $X_{i,G}$ will have a bigger contribution on the individual $U_{i,G+1}$.

In the algorithm, the variation factor and crossover probability which adjust adaptively can achieve the dynamic evolution of control parameters to obtain better optimization effect, and also reduce the influence caused by fixed setting.

2) The identification of precise fault location

The steps of precise fault location are:

① Assume that fault occurred in a point that x distance from the start point of the possible fault line, so it means a new $(n+1)^{th}$ node is added as the fault position.

② Revise the system impedance matrix, because the impedance matrix dimension changes from $3n \times 3n$ to $3(n+1) \times 3(n+1)$. Also the lengths of the lines also need to be change based on the distance x [8].

④ Calculate the fault feature value of the new $(n+1)^{th}$ node by assuming that the fault location is at the new node;

⑤ Use PADEA to automatically search the fault location with setting the fault distance x as variables and

choosing the fault feature value of the new node as fitness function.

When the searched fault point is closer to the actual fault point, the fitness function value is smaller. The final location result can be obtained when the fitness function value meets the required precision.

The flow chart of precise fault location is shown in Fig. 3.

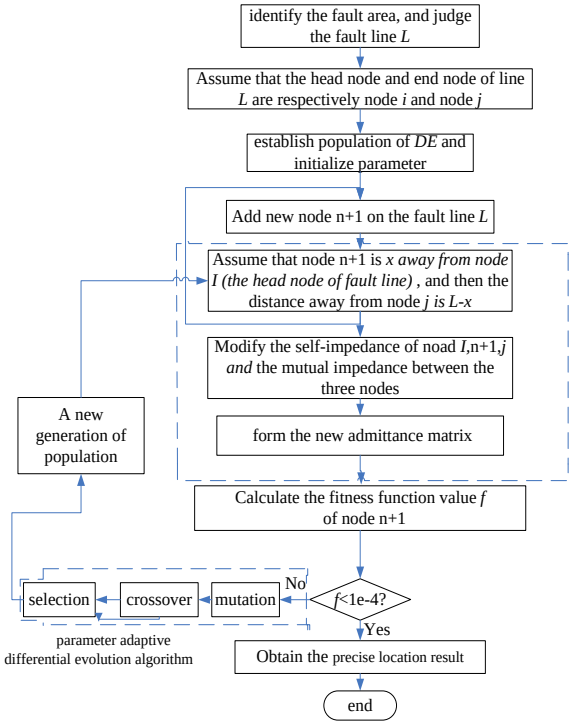

Fig. 3. Flow chart of precise fault location.

IV. Simulation and Verification

A. The Simulation Model

The method proposed in this paper is tested in an actual 10 KV substation AiDing in XinJiang. The simulation system model is built in Matlab/Simulink, while the topological structure is shown as Fig. 4. The total load is 3.6 MVA, the DG unit capacity and access point is shown in Table I, all the DG units account for 47% of the total load. The neutral points are grounded through Peterson coil. The line and load model respectively adopt π model and static constant impedance load model in Simulink.

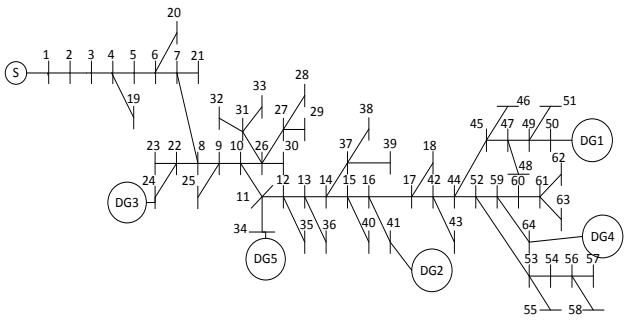

Fig. 4. The topology of simulation model.

TABLE I: The Capacity and Access Point of DG Unit

Name	Access point	Capacity /MVA	Name	Access point	Capacity /MVA
DG1	50	0.5	DG4	64	0.3
DG2	41	0.2	DG5	34	0.2
DG3	24	0.4			

B. Real-Time Extraction of Fundamental Wave Phase and Amplitude Based on STF

Firstly, plural state space description of single phase voltage can be built in MATLAB [10]. The initial parameters of STF are: state variable $\hat{x}_0 = \begin{bmatrix} 0 & 100\pi & 0 & 0 \end{bmatrix}^T$, estimation error covariance matrix $P_g = 10000 * eye(4,4)$, process noise covariance matrix $Q = 1e^{-5} * eye(4,4)$, measurement noise covariance matrix $R = 1e^{-3}$, forgetting factor $\rho = 0.95$, softening factor $\beta = 3$.

For taking signal fluctuation of the power system into account, the ability of tracking mutational states is shown as Fig. 5 when the system will gradually reach a steady state again after a single phase fault occurs at the 38th node during $t = 0.005 - 0.015s$.

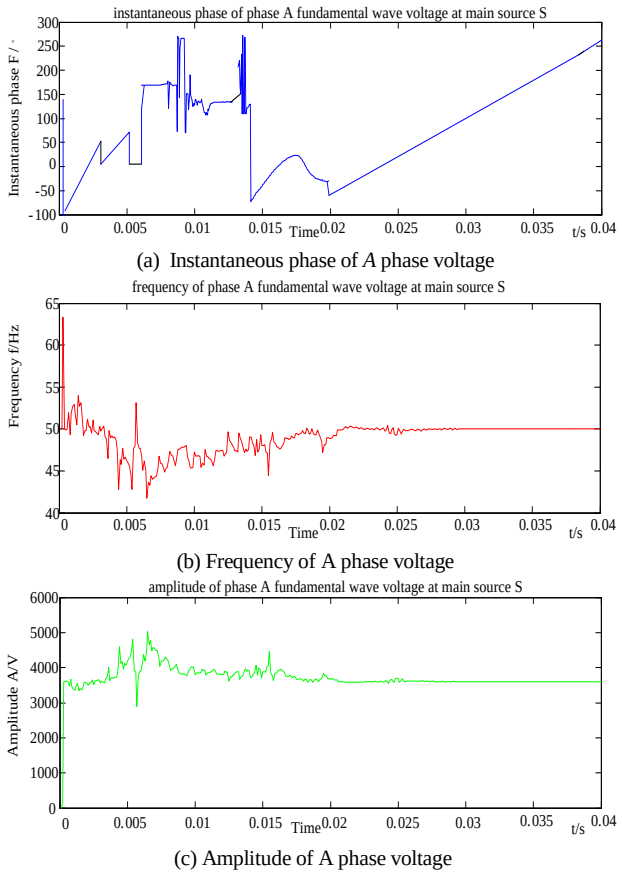

(a) Instantaneous phase of *A* phase voltage

(b) Frequency of A phase voltage

(c) Amplitude of A phase voltage

Fig. 5. The waveforms of STF when fault occurs at t=0.005~0.015s.

From Fig. 5, the parameters of the system will change and the tracking ability of STF will also become disordered when a fault occurs. STF can still track the phase, amplitude and frequency of fundamental wave voltage well

after the system gradually reaches a steady state again. The whole tracking process causes about half cycle to achieve smooth tracking state.

C. The Simulation Results of Fault Location Method

1) Fault area location results

Case 1: When a two-phase-grounding fault occurs at the 28th line, the fault feature value of each node shown in Fig. 6 can be calculated through MATLAB program according to the above analysis.

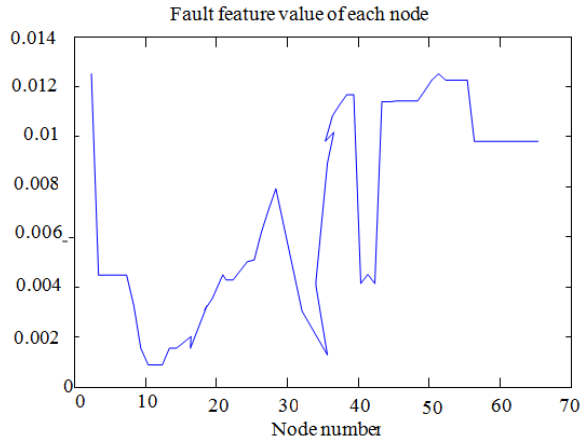

Fig. 6. Fault feature value of each node when two-phase grounding fault occurs at the 28th line

When a two-phase-grounding fault occurs at the 28th line, the three identified fault-associated nodes are respectively the 12th node, the 13th node and the 35th node. According to the node numbers, we can subsequently determine that the 28th line and the 29th line are the possible fault lines. The fault area can be located confidently.

Parts of the results of the fault area location are shown in Table II.

TABLE II: FAULT SECTION LOCATING RESULTS

Fault type	Fault line	Head node-end node	identified fault associated node	possible fault line
Two phase grounding	6	5-6	5,4,6	5,6
	15	9-25	9,25,8	14,15
	38	16-41	16,15,41	37,38
	40	17-18	17,18,42	40,41
	47	47-49	49,51,47	47,49
	46	45-47	47,48,45	45,46
Three phase grounding	49	49-51	49,51,47	47,49
	38	16-41	41,16,15	37,38
	7	6-20	6,20,7	7,8
	2	2-19	2,19,3	2,3
	12	22-23	22,23,7	11,12
	27	11-12	12,35,11	27,28
Single phase grounding	32	14-37	14,37,39	32,34
	6	5-6	5,6,20	6,7
	50	47-48	47,48,49	47,50

From Table II, we can see that the fault area location method based on Fig. 2 can identify the fault branch correctly. Quite a large number of simulations in our researches show that the method is effective for neutral non-grounded system, arc suppression coil grounded system and neutral directly grounded system.

TABLE III: THE RESULT OF PRECISE FAULT LOCATION

operation mode	Fault type	Fault line	Fault distance (km)	Judged fault line	Location Distance (km)	Absolute Error (m)	Relative Error (%)
directly grounded	Single phase grounding	32	1.2	32,34	1.1596	40.4	1.616
		17	2.14	17,19	2.0942	45.8	0.942
		6	1.3	6,7	1.2845	15.5	0.620
		50	1.4	47,50	1.4597	59.7	2.296
	Two phase grounding	48	2.7	48,49	2.6176	82.4	1.831
		10	1.6	9,10	1.7075	107.5	2.986
		2	1.5	2,3	1.4501	49.9	2.495
		27	1.4	27,28	1.3174	82.6	2.429
	Three phase grounding	13	2	12,13	2.0747	74.7	1.810
		41	1.5	40,41	1.4152	84.8	3.029
		7	1.7	6,7	1.6475	52.5	1.500
		49	1.84	47,49	1.7493	90.7	2.362
		26	2.5	26,27	2.3972	102.8	2.056
neutral non-grounded	Two phase grounding	6	1.2	5,6	1.1834	16.6	0.664
		15	1.8	14,15	1.9648	164.8	5.493
		28	1.8	28,29	1.9312	131.2	3.453
		38	1.6	37,38	1.7413	141.3	4.037
	Three phase grounding	40	1.9	40,41	1.8328	67.2	1.723
		47	1.4	47,49	1.2675	132.5	5.520
		60	1.2	60,61	1.4356	235.6	7.363
arc suppression coil grounded	Two phase grounding	49	2.1	47,49	1.9981	101.9	2.654
		38	1.7	37,38	1.8247	124.7	3.563
		41	1.4	41,42	1.4598	59.8	2.136
		7	1.8	7,8	1.6662	133.8	3.823
	Three phase grounding	2	1.8	2,3	1.7624	37.6	1.253
		12	1	11,12	1.1241	124.1	6.894
		27	1.8	27,28	1.9132	113.2	3.329
		19	0.9	17,19	0.7463	153.7	8.089

2) Fault precise location results

Then a precise fault location should be further achieved by utilizing a method, which is based on PADEA.

The obtained fault precise location results are shown in Table III.

From Table III, a number of simulation results show that the fault location method in distribution network with DG based on PADEA and the fault feature presented in this paper has high precision under three-phase impedance model. When the fault point is close to the main power supply, the result is better. The absolute error is within 100m. When the fault point is much farther away from the main power system, results are poorer, but the absolute error is within 400m. It is found in our research that the fault location effect are both correlated with the distance between fault line and the main power supply and with the grounding resistance.

Compared with traditional differential evolution algorithm, this paper mainly improves the parameter settings for the variation factor F and the crossover probability CR. Table IV shows the comparison results of the fault location through different algorithms.

TABLE IV: COMPARISON TABLE OF FAULT LOCATION RESULTS

Operation mode	Fault type	Fault line	Fault distance (km)	Fixed F and *CR*		Adaptive F and *CR*	
				Location Result (km)	Iterations	Location Result (km)	Iterations
Directly grounded	single phase grounding	1	1.5	1.4527	26	1.4544	22
	Two phase grounding	8 26	1.3 2.0	1.4197 1.7852	24 29	1.3785 1.8967	25 25
	Three phase grounding	3 41	1.4 1.5	1.2119 1.2987	28 48	1.2474 1.4152	28 36
Neutral non-grounded	Two phase grounding	6 15	1.2 1.8	1.0367 2.0801	38 42	1.1834 1.9648	31 40
	Three phase grounding	40 47	1.9 1.4	1.6548 1.0991	43 39	1.8328 1.2675	35 35
Arc suppression coil grounded	Two phase grounding	1 27	1.2 1.3	1.2016 1.1904	28 46	1.2001 1.2642	27 38
	Three phase grounding	12 28	1.0 1.6	1.2430 1.3761	38 43	1.1241 1.4595	32 35

From Table IV, the simulation results show that fault location method based on PADEA can achieve more precise fault location. Meanwhile, compared with the fixed parameter differential evolution algorithm PADEA can adjust the value of F and CR adaptively; obtain more accurate location result. Also the iteration number is decreased which means that the calculation time is shorter. This is because that it can adjust adaptively with the change of differential vector and better enrich the diversity of the variation vector. Also the crossover probability CR adjusts adaptively with the change of individual fitness value increment. CR will speed up the convergence under the condition of better fitness value.

V. CONCLUSION

This paper proposes a fault location method based on STF and PADEA for increasing the accuracy of fault location method. The fault area location method is adopted to search for the node with minimum fault feature value and locate the fault area after finishing the establishment of impedance model using the data calculated through STF. Then PADEA is applied to reduce the number of iterations and improve the location accuracy in the precise location section. Besides, this method can avoid the introduction of the asynchronous sampling error at measurement points and have a sound theoretical foundation. Simulation results in MATLAB/Simulink show that the method proposed in this paper has advantages of achieving high accuracy and better robustness.

REFERENCES

[1] X. X. Zhou, "To develop power system technology suitable to the need in 21stcentury,"*Power System Technology*, vol. 21, pp. 11-15, Nov. 1997.

[2] H. Zayandehroodi, A. Mohamed, H. Shareef, and M. Mohammadjafari, "Determining exact fault location in a distribution network in presence of DGs using RBF neural networks," in *Proc. IEEE International Conference on Information Reuse and Integration*, Las Vegas, 2011, pp. 434-438.

[3] K. P. Dash, K. A. Pradhan, and G. Panda, "An extended complex Kalman filter for frequency estimation of distorted signals," *IEEE Trans on Instrument and Measurement*, vol. 49, pp. 746-753, Sep. 2000.

[4] R. Storn and K. Price, "Differential evolution-a simple and efficient adaptive scheme for global optimization over continuous spaces," Technical Report International Computer Science Institute, Berkley, 1995.

[5] H. Xu, S. H. Miao, Z. Jiang, F. Zeng, L. Zhang, and P. Liu, "A new fault location algorithm based on fault component from finite synchronized phasor measurement unit," *Automation of Electric Power Systems*, vol. 2, pp. 43-48, Feb. 2013.

[6] L. C. Wang, Q. X. Li, X. Q. Liu, W. Zhang, and W. M. Pan, "Distribution network fault location based on the improved ant colony algorithm," *Power System Protection and Control*, vol. 22, pp. 29-33, Nov. 2008.

[7] Y. Chen, P. Jiang, Q. L. Wan, and S. Gao, *Power System Analysis*, Beijing: China Power Press, 2005, pp. 16-39.

[8] Z. J. Kang, A. Tian, and Z. Bai, "A fault area location method in distribution network with DG," *Telkomnika-Indonesian Journal of Electrical Engineering*, vol. 11, pp. 6870-6878, Nov. 2013.

[9] K. N. Song, S. Cong, K. Dcng, *et al*., "Design of adaptive strong tracking and robust kalman filter," in *Proc. 33rd Chinese Control Conference*, Nanjing, 2014, pp. 6626-6631.

[10] M. A. Shuai, R. Zhao, and X. B. Wu, "Strong tracking filter based fundamental phase real-time extraction for single-phase voltage," *Proceedings of the CSEE*, vol. 28, no. 28, pp. 83-89, Oct. 2012.
[11] G. Y. Li and M. G. Liu, "The summary of differential evolution algorithm and its improvements," in *Proc. 3rd International Conference on Advanced Computer Theory and Engineering*, Chengdu, 2010, pp. 3153-3156.
[12] M. F. Tasgetiren, P. N. Suganthan, T. J. Chua, and A. Al-Hajri, "Differential evolution algorithms for the generalized assignment problem," in *Proc. IEEE Congress on Evolutionary Computation*, Trondheim, 2009, pp. 2606–2613.
[13] S. B. Zhao, F. S. Zhang, J. Y. Zhong, and H. Tian, "An adaptive differential evolution algorithm and its application in reactive power optimization of power system," *Power System Technology*, vol. 6, pp. 169-174, June 2011.
[14] P. Guo, "Research on improvement of differential evolution algorithm," Ph.D. dissertation, Dept. Computer Science and Technology Tianjin University, Tianjin, China, 2012.
[15] L. Y. Jia and C. Zhang, "Self-adaptive differential evolution," *Journal of Central South University (Science and Technology)*, vol. 9, pp. 3759-3765, Sep. 2013.

Zhongjian Kang was born in Anyue, China in 1971. He received his bachelor degree from China University of Petroleum in 1993 and received his master degree and doctor degree from Harbin Institute of Technology in 1998 and 2001. Currently, he is a professor in the Department of Electrical Engineering of China University of Petroleum. Prof. Kang's research interests include Power system analysis and control, Power system fault detection and diagnosis, Oilfield automation equipment development and renewable energy generation control.

Ruiying Liu was born in 1990, she received her B.S. degree from China University of Petroleum in 2013.Now she is studying as a second grade postgraduate. Her research field focuses on electrical system design and fault detection and diagnosis.

Yanyan Feng was born in 1989, she received her B.S. degree from China University of Petroleum in 2011 and M.S. degree from China University of Petroleum in 2014.Her research field focuses on electrical system design and fault detection and diagnosis.